Channeling investigation of the crystalline structure of U_4O_{9-y}

Frédérico Garrido,[1,*] Lech Nowicki,[2] and Lionel Thomé[1]
[1]*Centre de Spectrométrie Nucléaire et de Spectrométrie de Masse, CNRS-IN2P3-Université Paris-Sud, Bâtiments 104-108, 91405 Orsay Campus, France*
[2]*The Andrzej Soltan Institute for Nuclear Studies, Hoża 69, 00-681 Warsaw, Poland*
(Received 30 June 2006; revised manuscript received 11 October 2006; published 22 November 2006)

The crystallographic structure of U_4O_{9-y} crystals can be described in terms of a spatial arrangement of special aggregates of oxygen atoms distributed throughout the basic fluorite framework of UO_2. The structure of U_4O_{9-y} single crystals was investigated with the ion-channeling method by recording angular scans across major crystallographic directions and along major atomic planes. Monte Carlo simulations were performed to interpret the channeling data. The presence of various anionic clusters previously proposed (such as the Willis-type 2:2:2 aggregate and Bevan-type cuboctahedral cluster), as well as more recent models involving the incorporation of extra oxygen atoms as oxo groups forming uranyl-type bonds and a structural disordering of part of the uranium sublattice, were investigated. Channeling data exhibit satisfactory agreement with both the Willis and Bevan-type aggregates. They are incompatible with the presence of a glassy part in the uranium sublattice and indicate that the presence of uranyl-type bonds is unlikely.

DOI: 10.1103/PhysRevB.74.184114 PACS number(s): 61.85.+p, 61.72.Ji, 61.66.−f, 61.18.−j

I. INTRODUCTION

Uranium oxides form one of the most numerous and complex families of binary metal oxides. From a structural point of view uranium oxides can essentially be divided into two groups: (i) low oxygen to uranium ratio, i.e., $O/U \in [2.0; 2.5]$, uranium oxides exhibit distorted *fluorite-type* structures based on the closed-packed fluorite arrangement of the uranium dioxide; (ii) high oxygen to uranium ratio, i.e., $O/U \in [2.5; 3.0]$, a *layerlike* configuration takes place, based on linear uranium-oxygen-uranium chains.[1–5] The fluorite-type structure is characterized by an extraordinary ability to accommodate oxygen atoms in interstitial positions caused by the clustering of oxygen defects. The formation of anionic aggregates was first postulated by Willis to account for neutron diffraction data obtained from both the disordered UO_{2+x} $(0<x<0.25)$ and the ordered U_4O_{9-y} $(0.02<y<0.06)$ phases.[6–10] The simplest model is the eponymous 2:2:2 Willis configuration of oxygen defects (involving two oxygen vacancies, two O′ atoms, and two O″ atoms). Each complex contains interstitial oxygen atoms displaced from the cubic-coordinated sites in the ⟨110⟩ and ⟨111⟩ directions, respectively, vacant normal oxygen sites, and either U(V) or U(VI) ions to maintain charge balance. More complex anionic clusters were also proposed, based on computer calculations, as well as specific ordering of clusters in linear arrays.[11–19] More recently, Bevan, Grey, and Willis demonstrated that the cuboctahedral cluster is the basic cluster defect in the $\beta-U_4O_{9-y}$ phase and that its presence is likely to occur in the UO_{2+x} phase.[20–24] Theoretical investigations of the presence of such clusters in U_3O_7 phases were examined recently and the clusters experimentally confirmed by neutron diffraction experiments.[25,26] In addition, the question of clustering of oxygen atoms in the UO_2-U_4O_{9-y} system was recently addressed by the use of x-ray absorption spectroscopy methods.[27,28] In marked contrast to previous experiments, the formation of oxo groups with small U-O distances associated with U(VI) and the surprising presence of a glassy part in the uranium sublattice were reported.

Three closely related phases of U_4O_{9-y} exist between room temperature and the triple point: the low-temperature α-U_4O_{9-y} phase is stable below 65 °C; the medium temperature β-U_4O_{9-y} phase is stable in the range 65–600 °C; the high temperature $\gamma-U_4O_{9-y}$ phase occurs above 600 °C.[29] Both the $\beta-U_4O_{9-y}$ and $\gamma-U_4O_{9-y}$ phases are cubic, whereas the $\alpha-U_4O_{9-y}$ phase is very slightly distorted to rhombohedral $(\alpha=90.078°)$.[30] The space group of the $\beta-U_4O_{9-y}$ phase and the $\gamma-U_4O_{9-y}$ phase is $I\bar{4}3d$, as is the $\alpha-U_4O_{9-y}$ phase if the rhombohedral distortion is neglected. U_4O_{9-y} exhibits long-range ordering with a superlattice containing $4\times4\times4$ fluorite cells. This phase is an ordered derivative of the disordered UO_{2+x} phase. The identification of the nature of anionic clusters in U_4O_{9-y} is of considerable importance since ordered structures normally contain the key to understanding their disordered parents, i.e., UO_{2+x} in the present case, and may also provide insights into the defect aggregation in other fluorite-based uranium oxides (such as U_3O_7 oxides).

The channeling of light particles in a crystalline material is a well established technique to investigate the structure of a solid and to quantify the local concentration of defects.[31,32] The channeling phenomenon occurs because atomic rows and planes steer incoming charged particles in the crystalline structure. The probability of close encounter of incoming particles with lattice nuclei is reduced by two orders of magnitude with respect to the cases of polycrystalline or amorphous matter. One of the most important applications of this technique concerns the lattice location of a diluted foreign element embedded in a crystalline structure. Development over the years of efficient computer simulation codes[33–38] describing the behavior of charged particles in a monocrystalline material allows us to extend the use of this technique to the study of more complex defect structures occurring in nonstoichiometric materials, and more specifically to the case of the anionic defect aggregates existing in anion-excess fluorite-related phases in the uranium-oxygen system.

The understanding of the complex structure of nonstoichiometric phases is classically investigated by diffraction

techniques, high resolution electron microscopy, and computer modeling.[39,40] However, serious difficulties arise in the determination of the complex cluster structures existing in anion-excess uranium oxides. Classical diffraction techniques provide information averaged over many unit cells and they are not fully adapted for the characterization of highly defective materials. Electron microscopy is playing an increasing role in studies on nonstoichiometry in the $UO_2-U_4O_{9-y}$ system. High resolution images of U_4O_{9-y} with a resolution approaching the atomic scale were recorded and tentatively interpreted in terms of the presence of cub-octahedral aggregates distributed within the fluorite-type matrix.[41] Conversely x-ray spectroscopic methods, sensitive to short-range order around each absorbing atom, give us a useful structural method directed toward the identification and localization of defect aggregates. In addition to the previously mentioned techniques, the channeling analysis presents a unique tool sensitive to both global distortions of atomic rows and planes, i.e., medium to long-range order, and atoms displaced off their regular crystallographic positions, i.e., short range order.[31,32] Therefore this duality of the channeling technique provides us with a complementary way to investigate the structure of defective materials at an intermediate scale between diffraction and spectroscopic methods.

The main objective of the present work is to examine by the channeling technique and computer simulation code the structure of the uranium sublattice and of the various oxygen clusters proposed in the literature for the structure of U_4O_{9-y}.

II. EXPERIMENTAL

U_4O_{9-y} single crystals were prepared by the method of oxygen transfer.[42–45] The principle is controlled oxidation of UO_2 single crystals into U_4O_{9-y} by the oxygen released by the thermal dissociation of U_3O_8 when both oxides are heated together in vacuum. Slices of crystalline UO_2 were cut from a large single crystal which had been oriented by x-ray back-reflection Laüe photography. One side of each UO_2 slice was mechanically polished down to 0.25 μm to produce a mirror finish. Samples were then annealed at 1400 °C in an Ar/H_2 (10%) reducing mixture in order to remove the damage induced by the polishing process and restore the stoichiometric composition. The starting U_3O_8 powder was heated at 500 °C under air to provide the exact stoichiometry O/U=2.667. Calculated amounts of stoichiometric UO_2 single crystals and U_3O_8 powders were then placed in an evacuated quartz tube and heated for one month at T=1100 °C. The final composition of samples was expected to be 2.243±0.001, i.e., in the homogeneity range for the U_4O_{9-y} phase.[44] The actual composition was determined by weight gain measurements performed on single crystals: 2.242±0.001. X-ray diffraction (XRD) analysis has demonstrated that the samples exhibit the characteristic features of the U_4O_{9-y} phase, i.e., the presence of super-lattice lines, due to the systematic displacements of uranium atoms to form a $4\times4\times4$ superstructure. The cell parameter is a =2.1768 nm, in agreement with reported values.[44]

The ion channeling backscattering technique was applied to investigate the crystalline structure of U_4O_{9-y} single crystals. Channeling experiments were performed using the ARAMIS facility[46] at the CSNSM-Orsay with a ^{4}He beam of 3.085 MeV energy in order to sense simultaneously both the U sublattice *via* backscattered ^{4}He ions from the U atoms and the O sublattice by the use of the ^{16}O (^{4}He,^{4}He) ^{16}O elastic scattering resonance occurring at 3.038 MeV.[47,48] Random backscattering spectra were recorded using a rotating random procedure with a tilt angle of 4° from the normal to the surface of the sample in order to avoid channeling effects. Angular scans were performed by means of a computer-controlled four-motor goniometer (two axes of rotation and x-y translation). Backscattered ^{4}He were registered in a silicon surface barrier detector located at 165°. The energy resolution of the experimental setup was 15 keV, corresponding to a depth resolution of about 10 nm.

The Monte Carlo MCCHASY code (developed at SINS Warsaw) was used to interpret channeling data.[38] The code was adapted to take into account very large and complex unit cells. Both the Monte Carlo method and the nuclear-encounter probability approach were applied.[33] The principle of this method lies in the accumulation of probabilities of close collisions of the projectiles (helium ions) with target nuclei when the projectiles pass through the crystalline structure in a direction close to a low-index axis. The crystal structure is treated as a sequence of monolayers. Interactions of the projectile with all atoms located within a 500-pm radius circle centered at the impact point are considered. Small changes of the vector of the projectile velocity are determined by assuming the Ziegler-Biersack-Littmark potential for the interaction between the projectile and target atoms[49] and by using the Gauss-Mehler quadratures.[50,51] Energy loss was calculated with the classical Lindhard approach:[52] half of the energy loss of a nonchanneled projectile is independent of its trajectory while the second half is proportional to the local concentration of electrons. Typically about 10^5 projectile trajectories are calculated in a single run of the code.

III. RESULTS

A. Composition of the sample

Random backscattering spectra recorded on UO_2 and U_4O_{9-y} single crystals are presented in Fig. 1. The spectra can be resolved into two signals: (i) the backscattering of ^{4}He ions from the U atoms located up to a depth of 2.5 μm; (ii) below ~1.1 MeV the signal of the ^{4}He ions from the O atoms is barely visible, except the presence of a small peak caused by the elastic scattering resonance on ^{16}O corresponding to atoms located at a depth 50–200 nm. The spectrum recorded on the U_4O_{9-y} sample exhibits a deficiency in the U backscattering yield with respect to the spectrum recorded on the UO_2 sample. Such a deficiency is attributed to the change in the energy loss of analyzing particles due to the incorporation of one extra oxygen atom per unit cell in U_4O_{9-y} compared to U_4O_8(i.e., UO_2). Fits to the experimental data performed by means of the RUMP code (Fig. 1) provide a quantitative evaluation of the composition of the U_4O_{9-y} sample, using the UO_2 sample as a reference and assuming that the Bragg rule for stopping power calculations is fulfilled.[53,54] The mean composition of the U_4O_{9-y} sample

estimated by this method is O/U=2.21±0.02, in fair agreement with the measured composition deduced from weight gain measurement O/U=2.242±0.001. The difference may be attributed to the accuracy in the calculation of stopping powers. Note that the surface of the sample (over a depth of ~30 nm) is overoxidized with a composition O/U~2.5 (see the small depletion in the U_4O_{9-y} random spectrum below the sample surface). An additional and independent determination of the sample composition (in the range 50–200 nm) was performed by integration of the resonance oxygen peak of the UO_2 and U_4O_{9-y} crystals. The precision of this method is limited by the high background produced mainly by the scattering from the U atoms, superimposed to the oxygen resonance. The composition of the U_4O_{9-y} crystal estimated by this method is O/U=2.3±0.1, in agreement with previous results.

B. Channeling analysis

Spectra recorded in the main ⟨110⟩ axis are also presented in Fig. 1 for both UO_2 and U_4O_{9-y} crystals. The yield of aligned spectra normalized to random ones in the surface region is displayed in the inset. Both spectra exhibit the presence of a surface peak corresponding to backscattered ions from the first monolayers. The aligned spectrum recorded on the UO_2 single crystal exhibits an excellent channeling behavior attested by a value of the minimum axial yield χ_{min} =0.012 and a very low dechanneling level versus increasing depth. The similar aligned spectrum recorded on the U_4O_{9-y} single crystal appears to be at variance with the UO_2 case. Indeed, although the minimum axial yield measured in the surface region of the sample is still low, χ_{min}=0.023, a much larger dechanneling level versus increasing depth is observed. Such a behavior is related to the progressive scattering of the incident ^{4}He ion beam from U atoms slightly displaced from regular positions in the fluorite matrix and to the presence of extra O atoms in the U_4O_{9-y} structure.

A structural analysis was performed by recording angular scans across the three major low-index directions of the single crystals: [110], [100], and [111]. The U signal was integrated from the surface of the sample (surface peak excluded) over a depth of 100 nm. The O signal was extracted from the strong background due to the U signal and it was integrated in the range 50–200 nm. Figure 2 display various angular scans recorded across the three major axes for UO_2 and U_4O_{9-y} crystals. Tables I and II summarize the values found for the minimum axial and planar yields for the various crystallographic directions investigated.

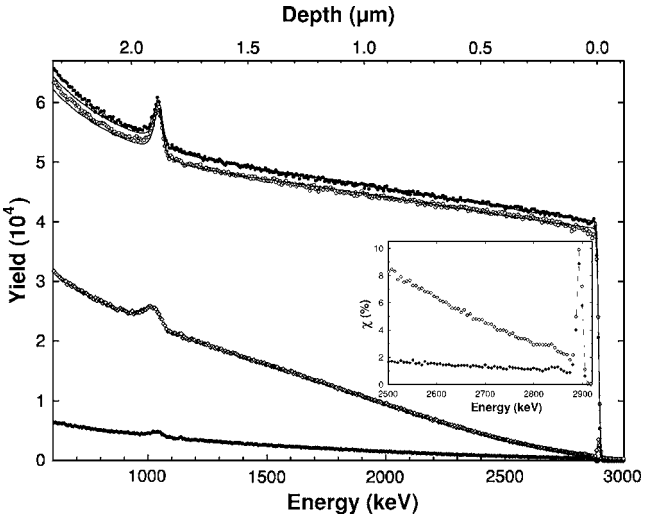

FIG. 1. RBS spectra recorded on ⟨110⟩-oriented UO_2 (full symbols) and U_4O_{9-y} (open symbols) single crystals in aligned (diamonds) and random (circles) directions. Solid lines are fits to random RBS spectra using the RUMP code (Ref. 53) and assuming samples of constant composition O/U=2.00 and O/U=2.21, which correspond to UO_2 and U_4O_{9-y} stoichiometries, respectively. Inset: details of normalized aligned spectra recorded on ⟨110⟩-oriented UO_2 and U_4O_{9-y} single crystals in the surface region.

Angular scans recorded on the UO_2 sample exhibit the characteristic features of a single crystal with the fluorite-type structure.[55–59] The dips are interpreted by considering both the large difference in the steering force acting on the probing ^{4}He ions between the two types of lattice atoms, due to the large difference in atomic numbers, and the variations in atomic structure along the various rows and planes:

(i) Along directions where atomic rows or planes are monoelemental (i.e., two separate sets of rows or planes, each consisting entirely of a single element)—e.g., ⟨110⟩, ⟨100⟩, {100}, {111}—the interaction of ions with lattice atoms exhibits a distinct orientation dependence for each sublattice. In this case the dips recorded on the U sublattice are much wider and deeper than those recorded on the O one due to the stronger steering action.

(ii) Along directions where atomic rows or planes are dielemental (i.e., containing both elements)—e.g., ⟨111⟩, {110}—the orientation dependencies for the interaction of the beam with U and O sublattices are identical. In such a case the much higher potential of U atoms governs the trajectory of analyzing particles along dielemental rows or planes and the role of O atoms is negligible.

TABLE I. Minimum aligned axial yields on UO_2 and U_4O_{9-y} single crystals for the various crystallographic directions investigated. The signal on U atoms was integrated over a depth of 100 nm. The resonance signal on ^{16}O atoms was integrated in the range 50–200 nm. The energy of the ^{4}He beam is 3.085 MeV.

	Uranium Sublattice		Oxygen Sublattice	
Axis	UO_2	U_4O_{9-y}	UO_2	U_4O_{9-y}
⟨100⟩	0.026	0.045	0.16	0.49
⟨110⟩	0.012	0.023	0.14	0.58
⟨111⟩	0.055	0.084	0.05	0.20

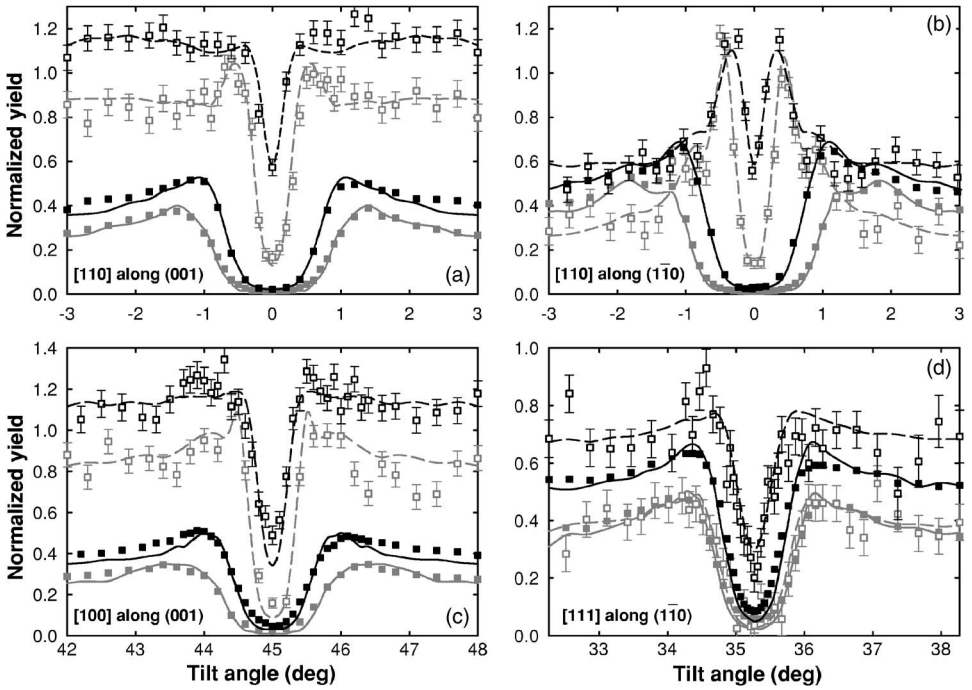

FIG. 2. Angular scans recorded on UO_2 and U_4O_{9-y} single crystals (a) across the [110] direction along the (001) plane; (b) across the [110] direction along the (1$\bar{1}$0) plane; (c) across the [100] direction along the (001) plane; (d) across the [111] direction along the (1$\bar{1}$0) plane. Black (gray) data and fits correspond to U_4O_{9-y} (UO_2). Full and open squares are data recorded on the U and O sublattices, respectively. Solid lines are fits to experimental data assuming (i) a defect-free UO_2 single crystal; (ii) the BGW model and parameters: q_U=1.8; q_O=2.0; r_O=308 pm (see Sec. IV B). Amplitudes of thermal vibrations are u_U (UO_2)=u_U (U_4O_{9-y})=6.5 pm and u_O (UO_2) =u_O (U_4O_{9-y})=9 pm. Tilt angles are defined with respect to the [110] direction.

Angular scans recorded on UO_2 were reproduced by performing Monte Carlo simulations assuming a defect-free UO_2 single crystal. It was assumed that both U and O atoms vibrate isotropically. A satisfactory agreement between experimental and calculated dips is obtained by setting the values of one-dimensional root-mean-square (rms) amplitudes of thermal vibrations u_U (UO_2)=6.5 pm and u_O (UO_2) =9 pm, for U and O sublattices, respectively (Fig. 2). Such values are in good agreement with the ones derived from neutron diffraction, x-ray spectroscopy techniques, and crystal dynamics.[8,27,28,60–63]

Scans recorded on the U_4O_{9-y} single crystal (Fig. 2) present the same basic features as those recorded on UO_2—since the basic fluorite framework is preserved—but they also exhibit striking differences for both sublattices:

(i) U scans recorded across the various axes and along both planes are much narrower than those recorded on UO_2. This strong reduction proves that a portion of the U atoms is displaced with respect to the ideal fluorite positions. As a matter of fact the influence of positions of O atoms on the shape of U scans can be neglected for the specific case of uranium oxides.[64] This observation is in agreement with systematic small displacements of U atoms from *fcc* positions evidenced by x-ray, neutron, and electron diffraction analyses.[8,20–24,29,30,65–79]

(ii) The channeling yield on U atoms in both investigated planes is largely enhanced with respect to UO_2 with typical values 0.40 and 0.45 for (001) and (1$\bar{1}$0) planes, respectively. Thus, both monoelemental {100} U planes as well as dielemental {110} planes are distorted due to displacements of U atoms in the U_4O_{9-y} crystal.

(iii) A strong increase in the minimum axial yield recorded on the O sublattice is evidenced with respect to UO_2, irrespective of the crystal orientation. Nevertheless a well pronounced dip is observed for the three main crystallographic directions, supporting the fact that the O sublattice is

TABLE II. Minimum planar yields on UO_2 and U_4O_{9-y} single crystals for the various crystallographic directions investigated. The signal on U atoms was integrated over a depth of 100 nm. The resonance signal on ^{16}O atoms was integrated in the range 50–200 nm. The energy of the ^4He beam is 3.085 MeV.

	Uranium Sublattice		Oxygen Sublattice	
Plane	UO_2	U_4O_{9-y}	UO_2	U_4O_{9-y}
{100}	0.25	0.40	0.85	1.15
{110}	0.35	0.45	0.30	0.60
{111}	0.25	0.35	1.0	1.25

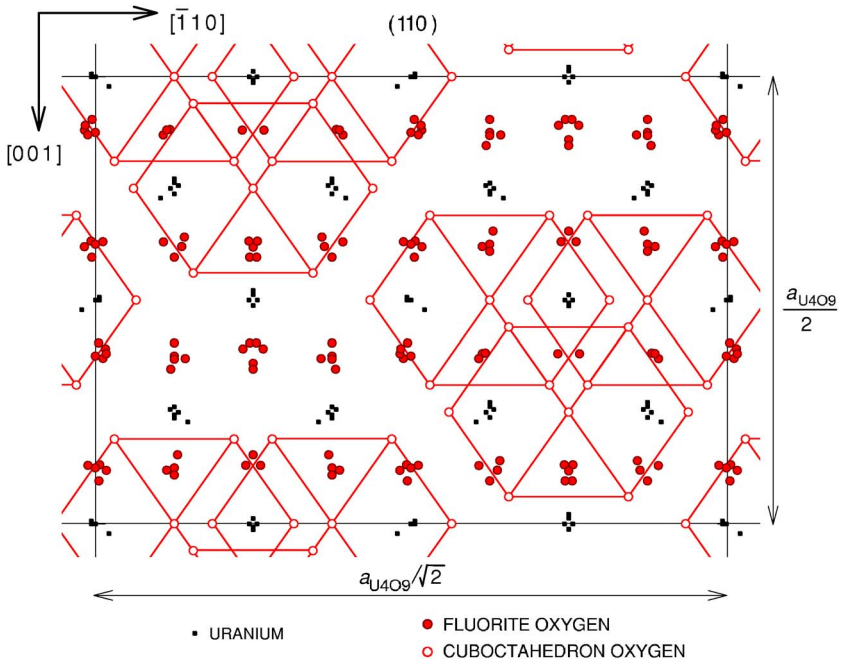

FIG. 3. (Color online) Two-dimensional unit cell of the (110) projection of $\beta-U_4O_{9-y}$. Edges of O cuboctahedra are represented by solid lines. For visualization purpose all displacements of atoms located near fluorite sites are twice as large as those specified in Table 4 of Ref. 24.

still very well organized. In particular, the large dip exhibited in the [110] direction differs from the absence of channeling in this direction previously reported by Matzke, Davies, and Johansson.[80]

(iv) A weak flux-peaking effect is observed for O along the monoelemental (001) plane with a typical value of 1.15. Due to the peculiar configuration of monoelemental O planes which are located at half distance between U planes, O atoms displaced from their regular ideal fluorite positions are exposed to the flux of channeled ions. Conversely, a very good channeling behavior is still present for O along the dielemental $(1\bar{1}0)$ plane. Both observations indicate that the major part of oxygen atoms still lie in these planes or are displaced only by a small distance from them. Since planar channeling sensed on the O sublattice is very sensitive to atomic disorder in both sublattices these results prove that the crystals possess a high degree of atomic ordering.

Angular scans recorded on U_4O_{9-y} were reproduced by performing Monte Carlo simulations (see Fig. 2) and the results are discussed in the following section.

IV. DISCUSSION

As aforementioned, analytical techniques investigating the long-range order of fluorite-type uranium oxides (such as x-ray, electron, and neutron diffraction techniques) and more local investigation techniques (such as x-ray absorption spectroscopy) give different pictures for the structure of oxygen-enriched uranium dioxide. In fact the structures of *both uranium and oxygen sublattices differ*. Long-range order techniques demonstrated that the *uranium sublattice* of uranium oxides in the range $UO_2-U_4O_{9-y}$ is only slightly affected by the incorporation of extra oxygen atoms.[6–10,20–24,29,30,65–79] In particular, the U_4O_{9-y} oxide forms a $4\times4\times4$ superstructure where U atoms are slightly displaced from their regular fluorite-type positions in a systematic pattern. The face-centered-cubic structure is thus essentially preserved. Figure 3 shows the projection on the (110) plane of the positions of U and O atoms according to the most recent diffraction experiments;[24] it evidences the systematic small displacements of U atoms from *fcc*-type positions. This description is challenged by a local investigation of the structure of those oxides by EXAFS.[27,28] Authors of this latter work proposed that a large fraction of the material remains largely intact (i.e., a UO_2-like crystal) while the remaining part is considered to be in a "spectroscopically silent glassy state." Similarly large differences in the *oxygen sublattice* between UO_2 and U_4O_{9-y} were evidenced. Both local and long range order techniques revealed that the extra oxygen atoms are incorporated into defect aggregates. Diffraction techniques indicated that O atoms form Willis-type or Bevan-type clusters characterized by rather long U-O bonds (typically 220–240 pm),[6–10,20–24,79] while local techniques prioritize oxo groups with typical short U-O distances (174 pm).[27,28] In this work, the validity of the various descriptions of the U_4O_{9-y} structure previously proposed is explored by the use of Monte Carlo simulations of channeling data. The various models are tested in the framework of two classes of descriptions: (i) a *statistical* description where U and O atoms are sited on regular or interstitial positions in the fluorite-type cell with a given probability for a given site; (ii) a *crystallographic* description where positions of atoms are derived from the space group of the model to be tested.

A. Statistical approach

In this approach, the average cell of the U_4O_{9-y} crystal is analyzed by assuming that U and O atoms are located at the UO_2 fluorite-type lattice and that extra O atoms are sited at well-defined places in the cell according to given probabilities. In such a description the long-range order (i.e., the superstructure) of the crystal is not taken into

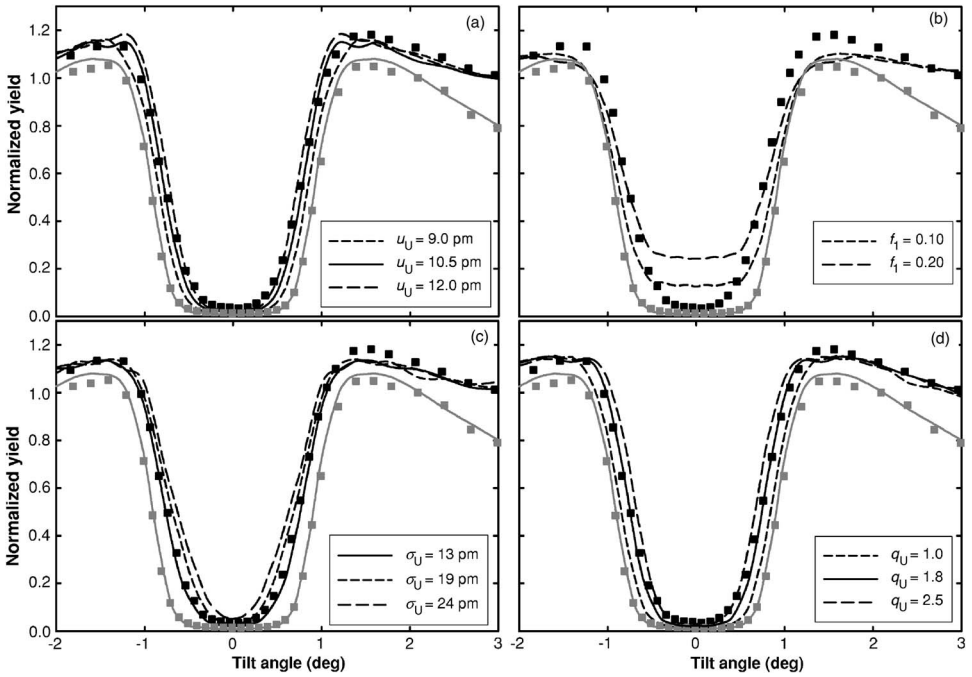

FIG. 4. Angular scan on the U sublattice recorded on a U_4O_{9-y} single crystal across the [110] direction at 13° from the $(1\bar{1}0)$ plane (black squares). Solid lines are fits to experimental data assuming that (a) the rms thermal vibrations of U atoms u_U (U_4O_{9-y}) are enlarged; (b) a fraction f_1 of U atoms is randomly dispersed in the structure and the remaining $(1-f_1)$ fraction is sited at fluorite-type positions; (c) 5/12 of U atoms are dispersed in the structure with a Gaussian distribution characterized by a standard deviation σ_U and the remaining 7/12 are sited at fluorite-type positions; (d) atoms are sited according to the BGW description with parameters: q_U; q_O=2.0; r_O=308 pm (see text). An angular scan on the U sublattice recorded on a UO_2 single crystal in the same conditions is plotted for comparison (gray squares); the solid line assumes a defect-free UO_2 single crystal. Amplitudes of thermal vibrations are u_U (UO_2)=u_U (U_4O_{9-y})=6.5 pm.

account. This drawback is not crucial for the interpretation of channeling data which are not sensitive to the presence of superstructures.

1. Investigation of the uranium sublattice

In uranium oxides the ion channeling in the crystal recorded on the U sublattice is essentially independent of the distribution of O atoms in the lattice.[38,64] As previously discussed in Sec. III, experimental U dips are much narrower in U_4O_{9-y} than in UO_2. Two structural models were attempted to quantitatively reproduce the differences between channeling angular scans recorded on UO_2 and U_4O_{9-y}. The common aim of the models was to reproduce the apparent "disorder" of the U sublattice in U_4O_{9-y} with respect to UO_2. In the first model, departures of U atoms from the *fcc* locations were reproduced by random displacements around these positions assuming a Gaussian distribution. In the second model it was assumed that U_4O_{9-y} is a mixture of two portions: an unaltered structure of UO_2 and a glassy component.

a. U atoms located at fluorite-type positions. A first tentative way to quantitatively reproduce the apparent disorder in the U sublattice, i.e., U displacements displayed in Fig. 3, is to enlarge the rms displacements of U atoms u_U (U_4O_{9-y}) from their regular sites to account for additional displacements exhibited by U atoms. In this approach both the static (atoms displaced from regular positions) and dynamic disorders (thermal vibrations) are fully accounted for by thermal vibrations alone. As apparent from Fig. 4(a), the best agreement between experimental and calculated angular scans is obtained when the amplitude of atomic vibrations is fixed at u_U (U_4O_{9-y})=10.5 pm. This value is close to the one deduced from neutron diffraction experiments performed on U_4O_{9-y} at room temperature u_U (U_4O_{9-y})=8.7 pm[8] and it should be compared to u_U (UO_2)=6.5 pm for regular UO_2.

b. Mixed crystalline and glassy model. In their work using EXAFS Conradson *et al.*[27,28] proposed that a large part of the U sublattice remains intact and that the remaining part is in a glassy state.

First Monte Carlo simulations were performed assuming that a given fraction f_1 of U atoms is *randomly* displaced in the structure while the remaining part $(1-f_1)$ of U atoms is still exactly located at ideal fluorite positions (as in UO_2). Thus, in this model the U disorder is entirely accounted for by the presence of amorphous zones in the sample. Fits to angular scans were performed assuming that the rms amplitude of thermal vibrations u_U (U_4O_{9-y})=6.5 pm (as in UO_2). As is apparent in Fig. 4(b) no agreement can be found between the low experimental value of the minimum axial yield and the narrowness of the angular scan, irrespective of the amorphous fraction f_1. It is worth noting that a similar disagreement is also obtained for other angular scans irrespective of the crystalline orientation. Besides it should be emphasized that the low value of the minimum axial yield in the O sublattice observed across every main crystalline direction provides additional evidence that the presence of an amorphous region is unlikely. Indeed the channeling behav-

ior of ions in fluorite-type uranium oxides is essentially governed by the U sublattice.[38,64] Thus any significant disordering of the U sublattice would lead to a strong increase in the values of the minimum axial yields, a feature which is not observed experimentally. The channeling results lead us to conclude that the structure of U_4O_{9-y} cannot be described by the presence of amorphous zones scattered in an unaltered UO_2 matrix.

In the description of U_4O_{9-y} proposed by Conradson *et al.*,[27,28] it is assumed that a given fraction f_2 of uranium atoms is spread around fluorite-type positions with a Gaussian distribution and that the remaining fraction $(1-f_2)$ consists of atoms located at ideal fluorite positions. Values provided by fits of EXAFS data serve us as starting values to reproduce angular scans.[27] A fraction $f_2=5/12$ was modified in the following way: 1 atom each is dispersed at ±24 pm and 1.5 atom each is dispersed at ±12 pm from the original fluorite-type positions, while the remaining fraction $(1-f_2)=7/12$ is unperturbed. Such distributions of U atoms dispersed from U rows were simulated by a Gaussian distribution characterized by a standard deviation σ_U. The rms amplitude of thermal vibrations was set to $u_U(U_4O_{9-y})=6.5$ pm. Fits to reproduce the lattice disorder in the U sublattice based on this description were performed by changing the standard deviation of the Gaussian distribution. A good agreement can be found between calculated and experimental dips assuming a value $\sigma_U=13$ pm [Fig. 4(c)]. This latter value is much lower than the displacements deduced from x-ray spectroscopy (in the range 19–24 pm) and it demonstrates once again that *U atoms are still located at or near fluorite-type positions*. Note that the present analysis is fully consistent with the one performed in Sec. IV A 1 a where all U atoms (i.e., $f_2=1$) are spread according to a Gaussian distribution (attributed to thermal vibrations) with a lower value of an equivalent standard deviation $\sigma_U=\sqrt{u_U^2(U_4O_{9-y})-u_U^2(UO_2)}=\sqrt{10.5^2-6.5^2}=8.2$ pm. Thus, although the presence of amorphous zones is excluded by the channeling analysis, the presence of U atoms randomly scattered at a small distance from regular U rows is compatible with channeling data.

The main conclusion that can be drawn from this analysis is that the U sublattice is only slightly affected by the incorporation of extra O atoms in the fluorite-type structure. This result corroborates previous investigations performed with a large class of experimental techniques.[8,20–24,29,30,65–82]

2. Investigation of the oxygen sublattice

In this section we investigate the presence of the main anionic oxygen cluster proposed in the literature.

a. O atoms located at Willis-type clusters. Here the structure of U_4O_{9-y} is interpreted in terms of the presence of Willis-type clusters. This classical description of U_4O_{9-y} assumes that the space group of the average cell is $F\bar{4}3m$.[8,79] Uranium atoms occupy the exact fluorite positions (as in UO_2), whereas oxygen atoms occupy three positions: ideal fluorite positions (a portion of those positions is not occupied), O′ atoms located at $(\frac{1}{2}+v, \frac{1}{2}+v, \frac{1}{2})$ positions, and O'' atoms located at $(\frac{1}{2}+w, \frac{1}{2}+w, \frac{1}{2}+w)$ positions. This model includes four free parameters: the two displacement parameters v and w of O′ and O″ atoms with respect to the octahedral position, respectively, and occupancies of those sites. To limit the number of free parameters in the analysis, occupancies were fixed to their theoretical values predicted by the pure 2:2:2 Willis-type cluster[10] (i.e., exactly two vacancies in the fluorite sublattice, two O atoms located at O′ positions, two O atoms located at O″ positions) and only positional parameters (i.e., v and w) were allowed to vary. Since, as discussed in Sec. IV A 1, experimental U dips are narrower in U_4O_{9-y} than in UO_2, the rms displacements of U atoms from their regular sites were enlarged to account for additional displacements exhibited by U atoms: $u_U(U_4O_{9-y})=10.5$ pm. Figure 5 show experimental and calculated O angular scans recorded across the [110] axis along the three major planes, namely (001), $(1\bar{1}0)$, and (111), for selected values of positional parameters (v,w). Fits to angular scans were performed assuming that the rms amplitude of thermal vibrations $u_O(U_4O_{9-y})=15$ pm, in agreement with data derived from neutron diffraction experiments performed at the same temperature.[8] If additional oxygen atoms are located at octahedral positions (corresponding to $v=w=0$), calculated dips systematically underestimate O normalized yields both in the axes and along (001) and $(1\bar{1}0)$ planes, whereas the calculation overestimates the yield in the (111) plane. These observations are consistent with the fact that extra O atoms sited at octahedral positions are located in both {100} U planes and in {110} dielemental planes, while they are located at mid distance from two {111} O planes. The angular scans confirm that extra O atoms are not located at octahedral positions, as it was originally postulated in pioneering works on U_4O_{9-y}.[65,67,83,84] When the amplitude of O displacements from the octahedral position increases, calculated axial and planar yields are drastically modified. It is worth mentioning that experimental dips recorded on O atoms off main crystallographic planes are not sensitive to the displacements of O′ and O″ atoms and thus provide no information on the positions of extra oxygen atoms in the U_4O_{9-y} crystal. Best fits to experimental data provide values of the displacement parameter in the range 0.10–0.15 for v and w deduced from data recorded along the three considered planes. Actually the best agreement averaged over the three investigated planes is obtained for $v=0.10$; $w=0.125$ – (see the Willis model in Fig. 6). Previous values reported for the positional parameters v and w extracted from neutron diffraction and EXAFS spectroscopy data on UO_{2+x} and U_4O_{9-y} crystals range from 0.10 to 0.14, and from 0.06 to 0.15, respectively, in excellent agreement with the present channeling investigation.[6–10,18,20,23,24,79,81,82]

b. On the presence of oxo groups. One of the most puzzling aspects of the description of Conradson *et al.*[27,28] is the presence of oxo groups, i.e., short U-O distances. The reported distance of those U-O bonds (174 pm) is characteristic of the so-called "uranyl groups" as they are observed in many U (VI) compounds and minerals with bond length in

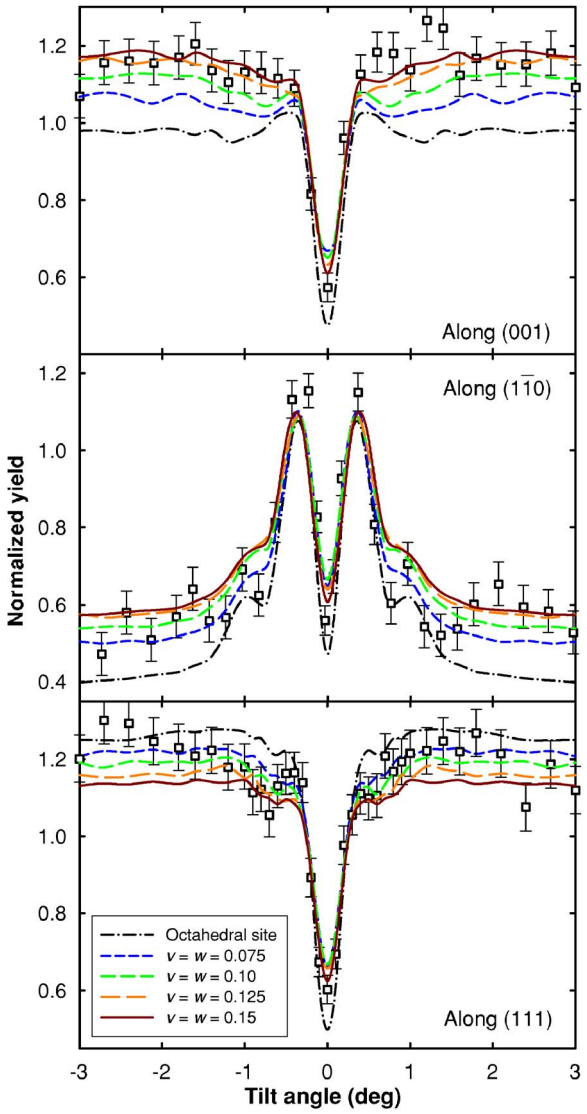

FIG. 5. (Color online) Angular scans on the O sublattice recorded on a U_4O_{9-y} single crystal across the [110] direction along the (001), (1$\bar{1}$0), and (111) planes. Lines are fits to experimental data assuming that U atoms are sited at ideal fluorite-type positions and that extra O atoms form Willis-type clusters characterized by the displacement parameters v and w. Amplitudes of thermal vibrations are u_U (U_4O_{9-y})=10.5 pm and u_O (U_4O_{9-y})=15 pm.

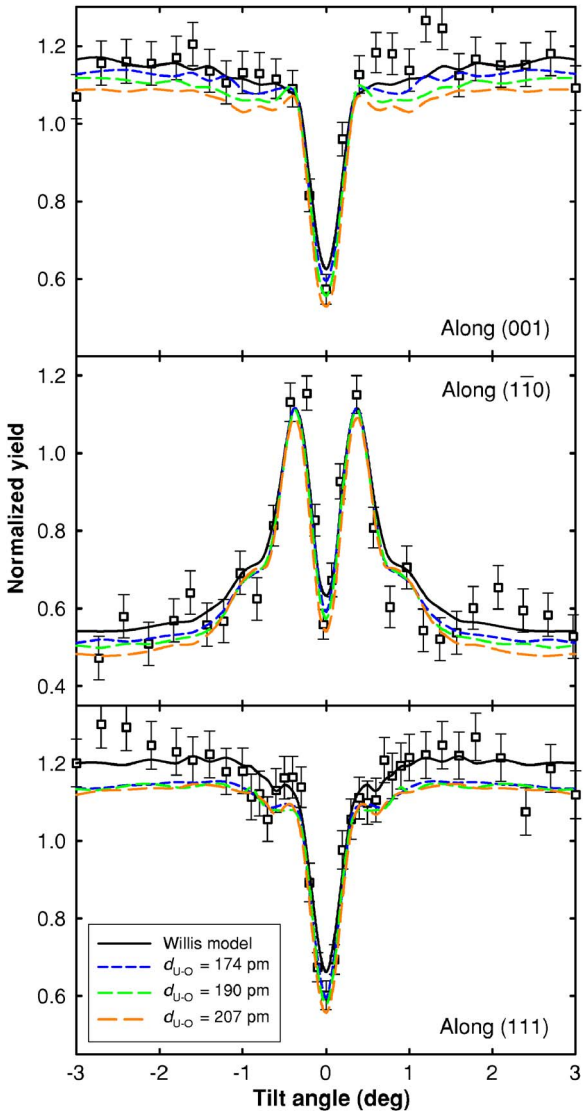

FIG. 6. (Color online) Angular scans on the O sublattice recorded on a U_4O_{9-y} single crystal across the [110] direction along the (001), (1$\bar{1}$0), and (111) planes. Lines are fits to experimental data assuming that U atoms are sited at ideal fluorite-type positions, extra O atoms are located at O′ sites and O″ atoms form oxo groups along ⟨111⟩-type directions characterized by the U-O distance d_{U-O}. Amplitudes of thermal vibrations are u_U (U_4O_{9-y})=10.5 pm and u_O (U_4O_{9-y})=15 pm.

the range 170–210 pm.[1–5,85] It is worth noting that they were never evidenced by diffraction techniques in distorted fluorite-type uranium oxides. Moreover the reported distance d_{U-O}=174 pm is considerably shorter than the characteristic distance U-O perpendicular to the equatorial planes in layered uranium oxides, e.g., in the U_3O_8 oxide, d_{U-O} =207 pm. Since those groups are thought to exist essentially as aperiodically disordered structures spread into the U_4O_{9-y} matrix, as evidenced by local techniques,[27,28] their tracking by the channeling technique was a major challenge. The uranyl group is characterized by strong covalent bonds with the uranium atom forming a linear unit and by the presence of extra ligands forming bonds within an equatorial plane perpendicular to the linear unit. The equatorial plane contains typically between four to six bonds. A credible mechanism for the formation of uranyl bonds in the fluorite-type structure is the displacement of two lattice oxygen atoms into short U-O groups along a ⟨111⟩-type direction. This scenario would require the concomitant distortion of the oxygen cube to create equatorial sites. The formation of uranyl bonds along ⟨111⟩-type directions is experimentally supported by the structural relationship existing between fluorite-type and layered-type uranium oxides evidenced during the oxidation of UO_2 single crystals into U_3O_8.[18,86–88] In the present work the presence of uranyl groups was explored by assuming that the totality of O″ atoms considered in the Willis model forms short uranyl U-O bonds along ⟨111⟩-type directions. Note

that the positions of the remaining displaced O atoms were constrained to be located at the O′ sites, as determined in the previous section, in agreement with both diffraction and x-ray spectroscopy techniques. The remaining O atoms are placed at fluorite-type positions. Thus, in this description, short U-O bonds along ⟨111⟩-type directions are randomly spread into the structure. Figure 6 compare best fits obtained by considering the Willis-type model (where $v=0.10$ and $w=0.125$) with those obtained by varying the distance corresponding to uranyl bonds. Such distances range from the pure uranyl distance reported in the UO_2^{2+} aqueous ion ($d_{U\text{-}O}=174$ pm) to the upper limit corresponding to the distance reported in layered-type uranium oxides ($d_{U\text{-}O}=207$ pm). Although agreements between experimental data and fits are poor for both (001) and $(1\bar{1}0)$ planes, the presence of uranyl groups cannot be ruled out on the basis of this sole set of data. A much better sensitivity is obtained when considering the channeling investigation performed along the (111) plane. The disagreement between experimental data and the simulation obtained along the (111) plane, whatever the investigated oxo distance, led us to the conclusion that the presence of a large amount of randomly dispersed uranyl groups oriented along ⟨111⟩-type directions in the crystal structure (typically one O atom per U_4O_{9-y} unit) is not compatible with our channeling data.

B. Crystallographic approach: Description in terms of the Bevan, Grey, and Willis model

The model of $\beta-U_4O_{9-y}$ proposed by Bevan, Grey, and Willis (referred to as the BGW model in the following) is to date the most accurate description of the crystallographic structure of this oxide.[20–24] It is therefore attractive to test this model against our experimental data. The crystal structure of U_4O_{9-y} is interpreted in terms of the BGW model based on the presence of ordered cuboctahedral clusters in the $4\times4\times4$ supercell structure with the space-group-type $I\bar{4}3d$. Although this model is strictly speaking limited to the β phase only (no fully satisfactory model has been proposed for the room-temperature α phase), recent neutron diffraction experiments revealed that similar cuboctahedral aggregates also exist in the α phase at room temperature.[89] The most precise description requires that each cluster exhibits $\bar{4}3m$ symmetry.[24] In this case, the number of positional parameters is too large (four positional variables for the U atoms and eight for the O atoms) for a quantitative estimation based on channeling measurements only. In order to limit the number of free parameters, three positional parameters, q_U, q_O, and r_O, were used to fit the angular scans. The values q_U and q_O correspond to the factors by which the U($a_{1\text{-}4}$) and O($b_{3\text{-}7}$) positional parameters were multiplied, respectively. Symbols a_i and b_i refer to the crystallographic positional parameters defined in Table 4 of Ref. 24. The parameter r_O is the radius of the oxygen cuboctahedron. By using such an approach the structural features of the BGW model are retained, while departures from the neutron diffraction investigation are to be determined by fitting q_U, q_O, and r_O against experimental channeling data. It should be pointed out that, in contrast to the description in terms of Willis-type clusters, in the present model the U sublattice is systematically distorted with respect to the fluorite-type structure. Since the channeling technique is not sensitive to the difference between static and dynamic disorders, the rms displacements of U and O atoms were fixed at the value obtained on UO_2 single crystals at the same temperature: u_U (U_4O_{9-y})=6.5 pm and u_O (U_4O_{9-y}) =9 pm. Parameters q_U, q_O, and r_O were refined against experimental angular dips recorded across the three main crystallographic axes. Best fits to experimental data are presented in Fig. 2. The influence of q_U on the width of U scans is dramatic, as shown in Fig. 4(d). U dips sketched in Fig. 2 are satisfactorily reproduced for the three main crystallographic directions assuming $q_U=1.8\pm0.1$. This result shows that the broadening of U rows in U_4O_{9-y} determined by the channeling technique is larger than the one derived from neutron diffraction analysis on $\beta-U_4O_{9-y}$. An in-depth investigation of the oxygen sublattice in the main [110] axis along (001), $(1\bar{1}0)$, and (111) planes was performed (Fig. 7) by exploring the influence of both q_O and r_O. In the case of the $(1\bar{1}0)$ plane, the variation of the width of O dips in the range $-1\leq\Psi\leq1$ is strongly influenced by q_O. Good agreement with experimental data is obtained by setting $q_O=2.0\pm0.2$. Figure 7 display the influence of the size of the oxygen cuboctahedron on the O yield. Although the influence of r_O in the central region of the O dip is almost negligible, its value imposes the O yield along the three investigated planes. The best fit deduced from the present analysis leads to $r_O=308$ pm. This value is slightly larger than the one deduced from the most recent neutron diffraction investigation performed on $\alpha-U_4O_{9-y}$ at room temperature: $r_O=299$ pm.[89]

C. Comparison of the various models

1. Uranium sublattice

The channeling properties of the uranium sublattice of U_4O_{9-y} are substantially the same as those of stoichiometric UO_2 (Fig. 2). U atoms are displaced from their fluorite-type positions but are still located near those positions. The analysis of channeling data excludes the presence of amorphous zones in the crystalline structure. Conversely, other descriptions are compatible with channeling data since U atoms are spread around fluorite-type positions (either in a statistical way or in a more sophisticated crystallographic description). It is clear from our analysis that the channeling technique *alone* cannot discriminate between these models for which the projections of U atoms on the plane perpendicular to the ion-beam direction are essentially the same. Nonetheless, the value of the atomic displacement parameter in the statistical description, u_U (U_4O_{9-y})=10.5 pm [Fig. 4(a)], which is much larger than the value u_U (UO_2)=6.5 pm derived from lattice-dynamic considerations[61] and from our channeling experiments, cannot be explained by thermal displacements alone and should be accounted for by the additional displacements of U atoms from the ideal fluorite positions. A similar conclusion was obtained for the mixed and glassy part model. Thus, the present channeling analysis confirms that

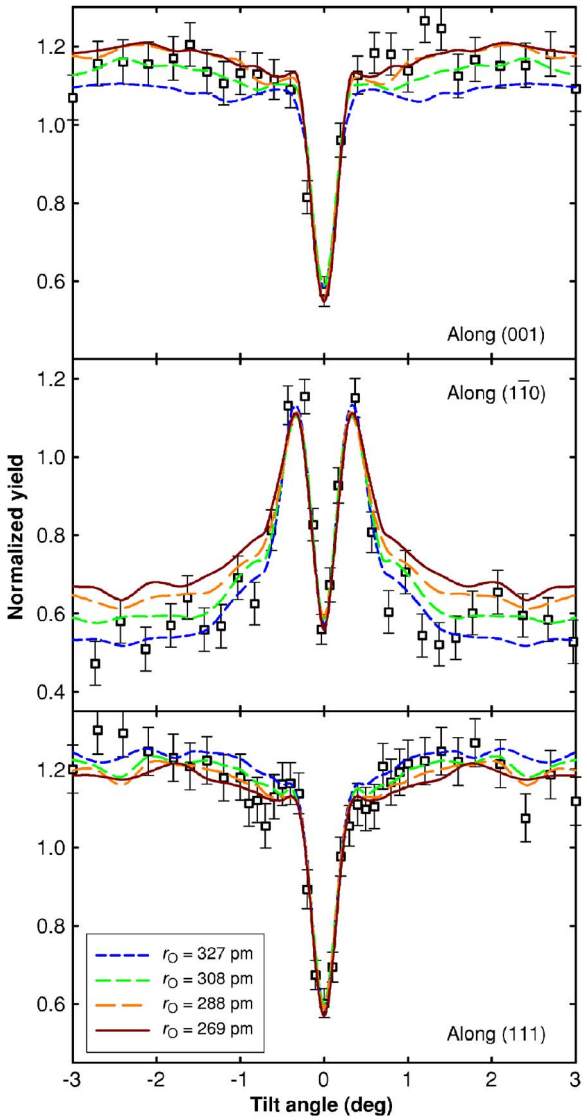

FIG. 7. (Color online) Angular scans on the O sublattice recorded on a U_4O_{9-y} single crystal across the [110] direction along the (001), (1$\bar{1}$0), and (111) planes. Lines are fits to experimental data assuming that U and O atoms are sited according to the BGW description. In this model extra O atoms form cuboctahedral clusters characterized by their radius r_O (positional parameters: q_U =1.8; q_O=2.0). Amplitudes of thermal vibrations are u_U (U_4O_{9-y}) =6.5 pm and u_O (U_4O_{9-y})=9 pm.

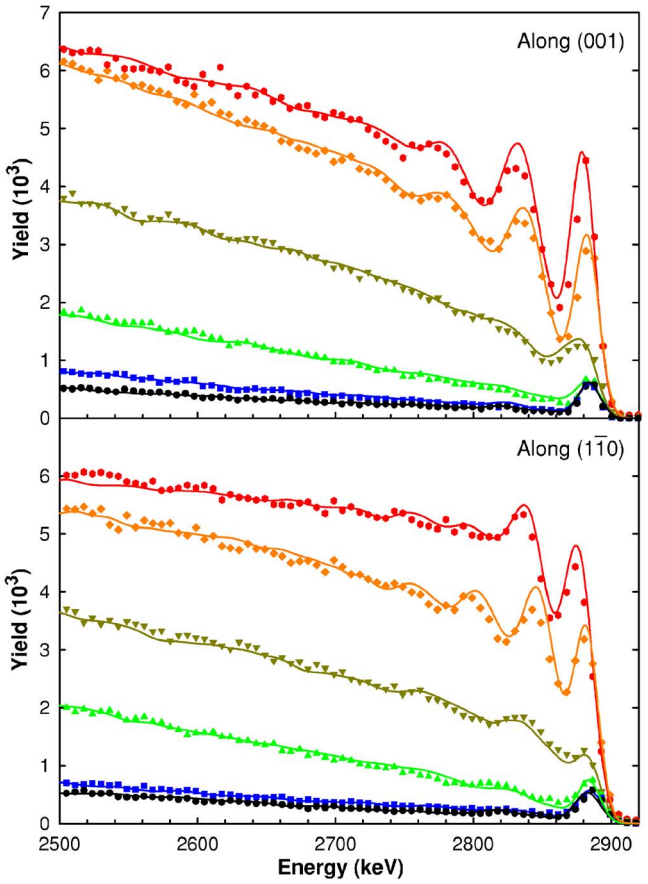

FIG. 8. (Color online) Experimental spectra recorded on a U_4O_{9-y} single crystal along the (001) and (1$\bar{1}$0) planes at selected values of the angle Ψ between the main crystallographic [110] direction and the ion-beam direction: Ψ=0° (circles); Ψ=0.2° (squares); Ψ=0.4° (triangles up); Ψ=0.6° (triangles down); Ψ =1.2° (hexagons); Ψ=3.0° (diamonds). Solid lines are fits to experimental data assuming the BGW model and parameters: q_U =1.8; q_O=2.0; r_O=308 pm. Amplitudes of thermal vibrations are u_U (U_4O_{9-y})=6.5 pm and u_O (U_4O_{9-y})=9 pm.

the BGW model is still the most accurate description of U_4O_{9-y} with respect to the U sublattice. This conclusion is additionally supported by the comparison of experimental and calculated spectra recorded at selected values of the angle between the main crystallographic direction and the ion-beam direction (Fig. 8). The excellent agreement obtained from the surface up to a depth of more than a half micrometer strengthens the arguments previously discussed and confirms once again the exactness of the BGW model.

2. Oxygen sublattice

The question of the nature of oxygen aggregates in U_4O_{9-y} is a matter of controversy. For the specific case of U_4O_{9-y} two major aggregates were proposed. The Willis-type cluster contains two anion vacancies, two ⟨110⟩ interstitial O atoms and two ⟨111⟩ interstitial O atoms. A larger cuboctahedron cluster involving twelve O atoms was proposed with the BGW model. As we discussed in Secs. IV A 2 and IV B, the channeling data recorded on the O sublattice are in good agreement with Monte Carlo simulations based on these two descriptions (Figs. 5 and 7). Nevertheless, the relationship between the positions of extra O atoms predicted by these two models should be emphasized. More precisely, the positions of the twelve O atoms forming the cuboctahedral arrangement coincide with the atomic positions of O′ interstitial atoms displaced along ⟨110⟩ in the average cell of the Willis model. Similarly the thirteenth O atom located inside the cuboctahedron is displaced along the ⟨111⟩ direction and corresponds to the O″ interstitial atoms displaced along ⟨111⟩ in the Willis model. Thus, the *main difference* between these two models lies in the huge reduction of the occupancy of O″ sites predicted by the BGW model with respect to the Willis model. Indeed the cuboctahedron cluster

contains twelve O′ for one O″ instead of one O′ for one O″ for the Willis-type cluster. The close connection between these two descriptions partially explains that satisfactory simulations of angular scans are obtained for both models (compare Figs. 5 and 7). In fact, the radius of the cuboctahedron is linked to the v parameter characteristic of the Willis aggregate by the relation: $r_O=0.25\sqrt{2}a(0.5-v)$, where a denotes the cell parameter. Thus, best agreements obtained for the Willis and the BGW models coincide since the value $v=0.10$ of the former model corresponds to $r_O=308$ pm for the latter one. Nonetheless, we must stress that several features of the channeling data strongly favor the cuboctahedral arrangement predicted by the BGW model versus the Willis model. As in the previous discussion regarding the U sublattice, the atomic displacement parameters obtained in the statistical description, u_O $(U_4O_{9-y})=15$ pm, is far larger than the one required from the BGW model, u_O $(U_4O_{9-y})=9$ pm, which is equal to the value derived for a defect-free UO_2 crystal. The latter value is analogous to values derived from diffraction experiments performed on U_4O_{9-y} crystals.[24] Secondly a careful analysis of angular scans performed along various planes (Figs. 5 and 7) shows that simulations performed on the basis of the Willis model reproduce the channeling level along planes but fail to reproduce the level in the axis. Simulations based on the BGW model fit the entire range of angle both in planes and in the axis.

Finally the essential question of the presence of oxo groups remains open. Our channeling data are not compatible with the presence of a large quantity of oxo oxygen atoms randomly located throughout the structure, typically one oxo atom for nine O atoms in U_4O_{9-y}. Due to the inherent limitation of the technique in terms of displaced oxygen atoms, the presence of some uranyl groups cannot be excluded on the basis of this channeling investigation. A typical amount of 5–20% of oxygen atoms forming uranyl groups can be inferred from the experiments of Conradson *et al.*[27] Although such a small amount cannot be excluded, all of our channeling data can be fully explained without considering uranyl bonds. This result confirms the absence of short U -O groups in U_4O_{9-y}, established very recently by the measurement of the neutron correlation functions.[90]

V. CONCLUSION

The present study demonstrates that the investigations of the structure of uranium oxides remain a compelling and controversial topic, notwithstanding a half-century of extensive research. The salient feature of this channeling work is that U_4O_{9-y} possesses a high degree of long-range atomic ordering which confirms that its structure, based on the fluorite-type UO_2 arrangement, is well organized for both U and O sublattices:

(i) The channeling data demonstrate that in U_4O_{9-y} the *fcc* uranium sublattice of UO_2 is essentially conserved with only small modifications in the U-U bond lengths, in agreement with results established by a large class of experimental techniques.[8,20–24,65–82] Conversely, the presence of a heterogeneous structure in the U sublattice, composed of a mixture of an intact UO_2-like phase and of a second glassy phase recently evidenced by x-ray absorption fine-structure spectroscopy (XAFS),[26,27] has to be excluded.

(ii) The rearrangement of the O sublattice due to the incorporation of extra O atoms in the UO_2 cell to form the U_4O_{9-y} structure was also investigated. Channeling data were successfully interpreted in terms of models in which extra oxygen atoms form either 2:2:2-type clusters (with displacement parameters $v=0.10$, $w=0.125$) or cuboctahedral aggregates (characterized by displacement parameters $q_U=1.8\pm0.1$, $q_O=2.0\pm0.2$, and cuboctahedron radius $r_O=308$ pm). Oxo groups, evidenced by XAFS spectroscopy at short U-O distances (in the range 170–210 pm),[27,28] i.e., shorter than those established by diffraction techniques (larger than 220 pm),[6–10,20–24,79] were not found.

In summary, the crystallographic description, proposed by Bevan, Grey, and Willis[20] on the basis of neutron diffraction experiments performed on $\beta-U_4O_{9-y}$, leading to an ordered arrangement of cuboctahedral antiprism-type clusters in the fluorite-type matrix, is the crystallographic model most compatible with our channeling data.

Finally, this work reports the contribution of channeling and associated computational techniques to the study of the nature of defect aggregates incorporated in nonstoichiometric compounds. In this respect, complex defect structures of several classes of materials may potentially benefit from the insight provided by this analytical technique, which can serve as a complementary tool to classical diffraction and spectroscopic methods. The highly controversial structure of U_3O_7 is currently being investigated, in order to discriminate between the various aggregates reported for this oxide.[1–5,25,26,78,81,82,91,92]

ACKNOWLEDGMENTS

Channeling measurements were performed at the ARAMIS facility at the CSNSM-Orsay. We are grateful to the staff for their assistance with the tandem accelerator. Oriented UO_2 single crystals would not have been so well prepared without the talent of Jacques Berthon at the Institut de Chimie Moléculaire et des Matériaux d'Orsay, Physico-Chimie de l'Etat Solide, Orsay Campus. We also express our gratitude to Adam Pietraszko at the Institute of Low Temperature and Structure Research of the Polish Academy of Sciences in Wrocław for the x-ray diffraction investigation of the superstructure of U_4O_{9-y} single crystals.

*Author to whom correspondence should be addressed. Electronic address: garrido@csnsm.in2p3.fr

[1] H. R. Hoekstra, Phase Relationship in the Uranium-Oxygen and Binary Oxide Systems, in *Uranium Dioxide: Properties and Nuclear Applications* (US Govt. Printing Office, Washington, DC, 1961), Chap. 6, p. 229.
[2] P. Pério, in *Nouveau Traité de Chimie Minérale*, Tome 15, Fascicule 2, edited by P. Pascal (Masson, Paris, 1961), p. 243; B. Belbeoch, in *Nouveau Traité de Chimie Minérale*, Tome 15, Fascicule 4, edited by P. Pascal (Masson, Paris, 1967), p. 558.
[3] E. H. P. Cordfunke, *The Chemistry of Uranium* (Elsevier, Amsterdam, 1969).
[4] *Gmelin Handbuch der Anorganischen Chemie*, Uran Erg.-Bd. Teil C1, System-Nummer 55 (Springer-Verlag, Berlin, 1977); Uran Erg.-Bd. Teil C2, System-Nummer 55 (Springer-Verlag, Berlin, 1977).
[5] J. J. Katz, G. T. Seeborg, and L. R. Morss, *The Chemistry of the Actinides* (Chapman & Hall, London, 1986).
[6] B. T. M. Willis, Nature (London) **197**, 755 (1963).
[7] B. T. M. Willis, Proc. Br. Ceram. Soc. **1**, 9 (1964).
[8] B. T. M. Willis, J. Phys. (Paris) **25**, 431 (1964).
[9] B. T. M. Willis, in *Thermodynamic and Transport Properties of Uranium Dioxide and Related Phases*, edited by C. E. Holley (IAEA, Vienna, 1965), Technical Reports Series No 39.
[10] B. T. M. Willis, Acta Crystallogr., Sect. A: Cryst. Phys., Diffr., Theor. Gen. Crystallogr. **34**, 88 (1978).
[11] A. K. Cheetham, B. E. F. Fender, D. Steele, R. I. Taylor, and B. T. M. Willis, Solid State Commun. **8**, 171 (1970).
[12] A. K. Cheetham, B. E. F. Fender, and M. J. Cooper, J. Phys. C **4**, 3107 (1971).
[13] C. R. A. Catlow, J. Phys. C **6**, L64 (1973).
[14] C. R. A. Catlow, Proc. R. Soc. London, Ser. A **353**, 533 (1977).
[15] G. C. Allen, P. A. Tempest, and J. W. Tyler, Nature (London) **295**, 48 (1982).
[16] G. C. Allen and P. A. Tempest, J. Chem. Soc. Dalton Trans. **1982**, 2169.
[17] G. C. Allen and P. A. Tempest, J. Chem. Soc. Dalton Trans. **1983**, 2673.
[18] G. C. Allen and P. A. Tempest, Proc. R. Soc. London, Ser. A **406**, 325 (1986).
[19] J. P. Goff, B. Fåk, W. Hayes, and M. T. Huchings, J. Nucl. Mater. **188**, 210 (1992).
[20] D. J. M. Bevan, I. E. Grey, and B. T. M. Willis, J. Solid State Chem. **61**, 1 (1986).
[21] B. T. M. Willis, J. Chem. Soc., Faraday Trans. 2 **83**, 1073 (1987).
[22] B. T. M. Willis, Adv. Ceram. **23**, 711 (1987).
[23] A. D. Murray and B. T. M. Willis, J. Solid State Chem. **84**, 52 (1990).
[24] R. I. Cooper and B. T. M. Willis, Acta Crystallogr., Sect. A: Found. Crystallogr. **60**, 322 (2004).
[25] L. Nowicki, F. Garrido, A. Turos, and L. Thomé, J. Phys. Chem. Solids **61**, 1789 (2000).
[26] F. Garrido, R. M. Ibberson, L. Nowicki, and B. T. M. Willis, J. Nucl. Mater. **322**, 87 (2003).
[27] S. D. Conradson, D. Manara, F. Wastin, D. L. Clark, G. H. Lander, L. A. Morales, J. Rebizant, and V. Rondinella, Inorg. Chem. **43**, 6922 (2004).
[28] S. D. Conradson, B. D. Begg, D. L. Clark, C. den Auwer, M. Ding, P. K. Dorhout, F. J. Espinosa-Faller, P. L. Gordon, R. G. Haire, N. J. Hess, R. F. Hess, D. W. Keogh, G. H. Lander, D. Manara, L. A. Morales, M. P. Neu, P. Paviet-Hartmann, J. Rebizant, V. Rondinella, W. Runde, C. D. Tait, D. K. Veirs, P. M. Villella, and F. Wastin, J. Solid State Chem. **178**, 521 (2005).
[29] K. Naito, J. Nucl. Mater. **51**, 126 (1974).
[30] B. Belbeoch and J.-C. Boivineau, Bull. Soc. Fr. Mineral. Cristallogr. **90**, 558 (1967); B. Belbeoch, J.-C. Boivineau, and P. Pério, J. Phys. Chem. Solids **28**, 1267 (1967).
[31] D. S. Gemmell, Rev. Mod. Phys. **46**, 129 (1974).
[32] L. C. Feldman, J. W. Mayer, and S. T. Picraux, *Materials Analysis by Ion Channeling: Submicron Crystallography* (Academic Press, New York, 1982).
[33] J. H. Barrett, Phys. Rev. B **3**, 1527 (1971).
[34] P. J. M. Smulders and D. O. Boerma, Nucl. Instrum. Methods Phys. Res. B **29**, 471 (1987).
[35] A. Dygo and A. Turos, Phys. Rev. B **40**, 7704 (1989).
[36] V. A. Khodyrev, V. Ya. Chumanov, K. K. Bourdelle, and G. P. Pokhil, Nucl. Instrum. Methods Phys. Res. B **94**, 523 (1994).
[37] A. Kling, Nucl. Instrum. Methods Phys. Res. B **102**, 141 (1995).
[38] L. Nowicki, A. Turos, R. Ratajczak, A. Stonert, and F. Garrido, Nucl. Instrum. Methods Phys. Res. B **240**, 277 (2005).
[39] D. J. M. Bevan, in *Comprehensive Inorganic Chemistry*, edited by J. C. Bailar, H. J. Emeléus, Sir R. Nyholm, and A. F. Trotman-Dickenson (Pergamon Press, Oxford, 1973), Vol. 4, p. 453.
[40] C. R. A. Catlow, in *Nonstoichiometric Oxides*, edited by O. T. Sorensen (Academic Press, New York, 1981), p. 61; L. Eyring, in *ibid.*, p. 337; A. K. Cheetham, in *ibid.*, p. 399.
[41] L. A. Bursill, P. J. Lin, D. J. Smith, and I. E. Grey, in *Proceedings of the Electron Microscopy and Analysis Group*, edited by G. Tatlock, IOP Conf. Proc. No. 78 (IOP, London, 1985), p. 463.
[42] W. Van Lierde and L. de Jonghe, Solid State Commun. **2**, 129 (1964).
[43] A. Kotlar, P. Gerdanian, and M. Dodé, J. Chim. Phys. Phys.-Chim. Biol. **64**, 862 (1967); **64**, 1135 (1967).
[44] W. Van Lierde, J. Pelsmaekers, and A. Lecocq-Robert, J. Nucl. Mater. **37**, 276 (1970).
[45] N. Masaki and T. Ishii, J. Cryst. Growth **6**, 207 (1970).
[46] E. Cottereau, J. Camplan, J. Chaumont, R. Meunier, and H. Bernas, Nucl. Instrum. Methods Phys. Res. B **45**, 293 (1990).
[47] A. Turos, Hj. Matzke, J. Chaumont, and L. Thomé, Nucl. Instrum. Methods Phys. Res. B **66**, 280 (1992).
[48] Z. Y. Zhou, Y. Y. Zhou, Y. Zhang, W. D. Xu, G. Q. Zhao, J. Y. Tang, and F. J. Yang, Nucl. Instrum. Methods Phys. Res. B **100**, 524 (1995).
[49] J. F. Ziegler, J. P. Biersack, and U. Littmark, *The Stopping and Range of Ions in Solids*, edited by J. F. Ziegler (Pergamon, New York, 1985), Vol. 1.
[50] Z. Kopal, *Numerical Analysis* (Wiley, New York, 1961).
[51] A. Dygo and A. Turos, Radiat. Eff. Lett. Sect. **85**, 237 (1985).
[52] J. Lindhard, K. Dan. Vidensk. Selsk. Mat. Fys. Medd. **34**, 14 (1965).
[53] L. R. Doolittle, Nucl. Instrum. Methods Phys. Res. B **9**, 344 (1985); **15**, 227 (1986).
[54] W.-K. Chu, J. W. Mayer, and M.-A. Nicolet, *Backscattering Spectrometry* (Academic Press, New York, 1978).
[55] L. Ericksson and J. A. Davis, Ark. Fys. **39**, 439 (1969).
[56] C. Cohen, Thèse de Doctorat d'Etat, Université Paris 7 (1973).
[57] F. Garrido, C. Choffel, J.-C. Dran, L. Thomé, L. Nowicki, and A. Turos, Nucl. Instrum. Methods Phys. Res. B **127–128**, 634 (1997).
[58] L. Nowicki, A. Turos, F. Garrido, C. Choffel, L. Thomé, J. Jagiel-

ski, and Hj. Matzke, Nucl. Instrum. Methods Phys. Res. B **136–138**, 447 (1998).
[59] F. Garrido, C. Choffel, L. Thomé, J.-C. Dran, L. Nowicki, A. Turos, and J. Domagala, Nucl. Instrum. Methods Phys. Res. B **136–138**, 465 (1998).
[60] B. T. M. Willis, Proc. R. Soc. London, Ser. A **274**, 134 (1963).
[61] G. Dolling, R. A. Cowley, and A. D. B. Woods, Can. J. Phys. **43**, 1397 (1965).
[62] B. T. M. Willis and R. G. Hazell, Acta Crystallogr., Sect. A: Cryst. Phys., Diffr., Theor. Gen. Crystallogr. **36**, 582 (1980).
[63] P. Ruello, L. Desgranges, G. Baldinozzi, G. Calvarin, T. Hansen, G. Petot-Ervas, and C. Petot, J. Phys. Chem. Solids **66**, 823 (2005).
[64] A. Turos, O. Meyer, L. Nowicki, J. Remmel, and M. Wielunski, Nucl. Instrum. Methods Phys. Res. B **85**, 448 (1994).
[65] B. Belbeoch, C. Piekarski, and P. Pério, Bull. Soc. Fr. Mineral. Cristallogr. **83**, 206 (1960).
[66] S. Steeb, Naturwiss. **47**, 465 (1960).
[67] B. Belbeoch, C. Piekarski, and P. Pério, Acta Crystallogr. **14**, 837 (1961).
[68] S. Steeb, J. Nucl. Mater. **3**, 235 (1961).
[69] S. Steeb and P. Mitch, J. Nucl. Mater. **15**, 81 (1965).
[70] H. Blank and C. Ronchi, Acta Crystallogr., Sect. A: Cryst. Phys., Diffr., Theor. Gen. Crystallogr. **24**, 657 (1968).
[71] K. Naito, T. Ishii, Y. Hamaguchi, and K. Oshima, Solid State Commun. **5**, 349 (1967).
[72] N. Masaki and K. Doi, Acta Crystallogr., Sect. B: Struct. Crystallogr. Cryst. Chem. **24**, 1393 (1968).
[73] T. Ishii, K. Naito, and K. Oshima, Solid State Commun. **8**, 677 (1970).
[74] T. Ishii, K. Naito, K. Oshima, and Y. Hamaguchi, J. Phys. Chem. Solids **32**, 235 (1971).
[75] N. Masaki and K. Doi, Acta Crystallogr., Sect. B: Struct. Crystallogr. Cryst. Chem. **28**, 785 (1972).
[76] K. Naito, T. Tsuji, and T. Matsui, J. Nucl. Mater. **48**, 58 (1973).
[77] N. Masaki, J. Appl. Crystallogr. **7**, 247 (1974).
[78] N. Masaki, J. Nucl. Mater. **101**, 229 (1981).
[79] J.-P. Lauriat, G. Chevrier, and J.-X. Boucherle, J. Solid State Chem. **80**, 80 (1989).
[80] Hj. Matzke, J. A. Davies, and N. G. E. Johansson, Can. J. Phys. **49**, 2215 (1971).
[81] D. J. Jones, J. Rozières, G. C. Allen, and P. A. Tempest, J. Phys. (Paris), Colloq. **47**, C8-745 (1986).
[82] D. J. Jones, J. Rozières, G. C. Allen, and P. A. Tempest, J. Chem. Phys. **84**, 6075 (1986).
[83] K. B. Alberman and J. S. Anderson, J. Chem. Soc. **1949**, S303.
[84] J. Hering and P. Pério, Bull. Soc. Chim. Fr. **19**, 351 (1952).
[85] P. C. Burns, R. C. Ewing, and F. C. Hawthorne, Can. Mineral. **35**, 1551 (1997).
[86] G. C. Allen, P. A. Tempest, and J. W. Tyler, Philos. Mag. B **54**, L67 (1986).
[87] G. C. Allen, P. A. Tempest, and J. W. Tyler, J. Chem. Soc., Faraday Trans. 1 **83**, 925 (1987).
[88] G. C. Allen and N. R. Holmes, J. Nucl. Mater. **223**, 231 (1995).
[89] F. Garrido, R. M. Ibberson, L. Nowicki, and B. T. M. Willis (to be published).
[90] F. Garrido, A. C. Hannon, R. M. Ibberson, L. Nowicki, and B. T. M. Willis, Inorg. Chem. **45**, 8408 (2006).
[91] H. R. Hoekstra, S. Siegel, and P. Charpin, J. Inorg. Nucl. Chem. **30**, 519 (1968).
[92] H. R. Hoekstra, S. Siegel, and F. X. Gallagher, J. Inorg. Nucl. Chem. **32**, 3237 (1970).